Deep cycle turbulence in Atlantic and Pacific cold tongues

James N. Moum[1], Kenneth G. Hughes[1], Emily L. Shroyer[2], William D. Smyth[1], Deepak Cherian[3], Sally J. Warner[4], Bernard Bourlès[5], Peter Brandt[6,7], Marcus Dengler[6]

[1]College of Earth, Ocean, and Atmospheric Sciences, Oregon State University, Corvallis Oregon USA
[2]Office of Naval Research, Arlington, VA, USA
[3]National Center for Atmospheric Research, Boulder CO USA
[4]Departments of Physics and Environmental Studies, Brandeis University, Waltham MA USA
[5]Institut de Recherche pour le Développement, Brest France
[6]GEOMAR Helmholtz Centre for Ocean Research Kiel, Kiel Germany
[7]Kiel Unviversity, Kiel Germany

Key Points:

- massive turbulence data sets from multiyear time series at sites in Pacific and Atlantic cold tongues are compared
- diurnal composites document similarities in variability and magnitudes of deep cycle turbulence in Atlantic and Pacific cold tongues
- a depth/amplitude scaling collapses turbulence dissipation measurements at three cold tongue sites to within a factor of 2

Corresponding author: J.N. Moum, `jim.moum@oregonstate.edu`

Abstract

Multiyear turbulence measurements from oceanographic moorings in the equatorial Atlantic and Pacific cold tongues reveal similarities in deep cycle turbulence (DCT) beneath the ML and above the core of the Equatorial Undercurrent (EUC). Diurnal composites of turbulence kinetic energy dissipation rate, ϵ, clearly show the diurnal cycles of turbulence beneath the ML in both cold tongues. Despite differences in surface forcing, EUC strength and core depth, DCT persists at all three sites, and is consistent between the sites. Time-mean values of ϵ at 30 m depth are nearly identical at all three sites. Variations of averaged values of ϵ in the deep cycle layer below 30 m range to a factor of 10 between sites. A proposed scaling in depth that isolates the deep cycle layers and of ϵ by the product of wind stress and current shear collapses vertical profiles at all sites to within a factor of 2.

Plain Language Summary

The equatorial cold tongues are large areas of the ocean that extract a globally disproportionate amount of heat from the atmosphere, and where that heat is mixed downward to the deeper ocean, a critical process in climate regulation. This mixing is dominated by deep cycle (DC) turbulence, a well-documented feature of the central equatorial Pacific cold tongue. Away from the equator, nighttime cooling of the sea surface causes increases in turbulence to the depth of the ML, typically a few tens of meters, below which turbulence is much reduced. On the equator, in contrast, opposing currents at the surface and roughly 100 m below the surface create a dynamic environment in which nightly increases in turbulence occur over many tens of meters below the ML base. This has been termed DC turbulence. Here, using massive data sets from both Pacific and Atlantic cold tongues, we show that DC turbulence is a persistent feature at each location and its main characteristics are consistent between them.

Index Terms

- Turbulence, diffusion, and mixing processes 4568
- ENSO 4522
- Equatorial oceanography 4231
- Diurnal, seasonal, and annual cycles 4227
- Time series experiments 4277

1 Introduction

Typically, open ocean surface mixed layers away from the equator are driven by a combination of wind stress and convection from nighttime cooling or other forms of cold air outbreaks (Shay & Gregg, 1986) and these mixed layers largely contain the turbulence within (Anis & Moum, 1994). A unique aspect of equatorial small-scale fluid dynamics that has been observed in the Pacific's cold tongue (PCT) at 0°140°W is the existence of diurnally-varying turbulence *beneath* a nighttime surface mixed layer (Moum et al., 1989; Lien et al., 1995). This sub-mixed layer turbulence at the equator has been termed deep cycle (DC) turbulence.

The existence of DC turbulence is linked to the strongly sheared current system above the core of the Equatorial Undercurrent (EUC) where the gradient Richardson number (Ri) persistently maintains a near-critical state with values fluctuating around 0.25 (Smyth & Moum, 2013), a state of marginal instability (MI). This persistent MI state is nudged beyond critical toward the end of the solar day, associated with the deepening of the sheared base of the diurnal warm layer that forms during the period of net daytime heating and deepens by shear-induced mixing (K. G. Hughes et al., 2021). A di-

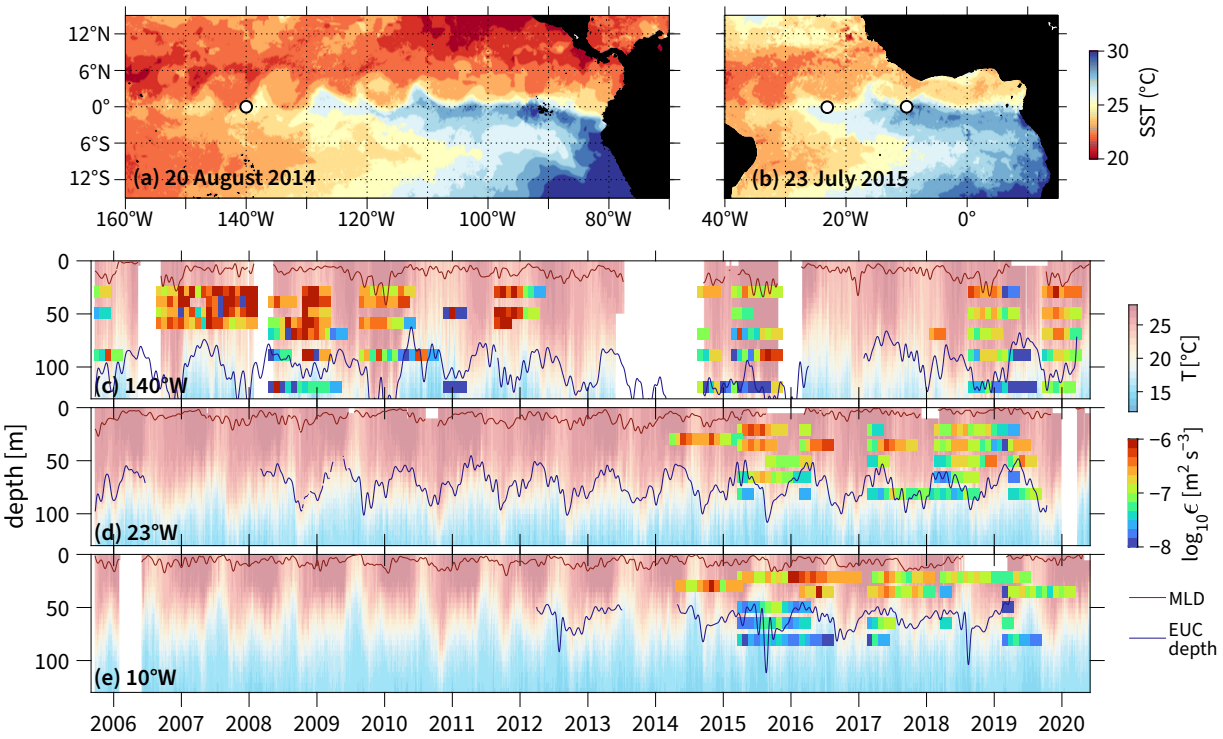

Figure 1. Measurements from χpod deployments in the (a) Pacific and (b) Atlantic cold tongues. Time series at (c) 140°W, (d) 23°W and (e) 10°W show colored bars (from monthly averages) to represent turbulence kinetic energy dissipation rate, ϵ. Background color is temperature (T). Solid white areas indicate lost moorings. Thin red line is the mixed layer (hereafter ML) depth defined as the depth at which T is smaller by 0.015°from its value at 1 m. Thin blue line is depth of EUC core.

urnal composite derived from 8 days of microstructure profiling revealed that the shear layer descends from near the surface to about 60 m at a rate close to 6 meters per hour (Smyth et al., 2013). The arrival of the shear layer was found to trigger shear instability and also to immediately precede enhanced turbulence, suggesting causality.

To summarize, DC turbulence has two defining properties:

(1) it occurs below the ML base, and
(2) it cycles diurnally.

This contrasts with, for example, turbulence below the ML created by near-inertial wave shear following wind events away from the equator, as such turbulence does not vary diurnally (Dohan & Davis, 2011; Hummels et al., 2020). Shipboard profiling measurements in the equatorial Pacific (Gregg et al., 1985; Moum & Caldwell, 1985; Moum et al., 1989) reveal both of the defining DC properties, albeit over only the cruise periods (typically a few weeks) and only when profiling was rapid enough to resolve the diurnal cycle. Both shortcomings are addressed using moored measurements.

From hourly-averaged mooring data that did not include turbulence measurements, Pham et al. (2017) showed the existence of the MI state below the ML base, varying diurnally with nighttime minima of Ri, in all seasons over the 9-year period 1998–2007. In lieu of direct microstructure measurements, they conducted large-eddy simulations,

with observationally-based initial and boundary conditions, to confirm that the observed MI state was indicative of turbulence. Daily-averaged mooring data can test for property (1), but not (2). Taking advantage of the greater availability of daily-averaged data, Pham et al. (2017) showed that the MI state existed in the PCT in all seasons over the 20-year period 1990–2010, confirming the persistence of property (1).

In the ACT, Hummels et al. (2013) documented property (1) by combining shipboard data taken at various times and locations. However, Hummels et al. (2013) did not find a clear diurnal cycle (property 2) in the ACT, likely due to limited data availability.

Moored turbulence measurements using χpods (Moum & Nash, 2009) have time resolution sufficient to resolve property (2) and now also extend over many years at a few sites. Data from the χpods at 140°W has shown how the DC varies with the El Nino-Southern Oscillation (ENSO) cycle and is a fundamental part of the underlying Bjerknes feedback (Warner & Moum, 2019) that governs transitions between ENSO phase states.

In the present analysis, we use the several years of moored records of turbulence from χpods at 0°140°W in the PCT (Moum & Nash, 2009), together with two sites in the ACT (Figure 1) to extend our knowledge of the DC by showing that

- property 2 (diurnal cycling below the ML) exists in both the ACT and the PCT;
- property 2 is a persistent feature in diurnally-composited distributions from measurements made over periods of many years;
- the amplitude and timing of DC turbulence varies with depth and longitude;
- a scaling of turbulence dissipation by the product of wind stress and current shear, combined with a depth scaling that isolates the DC depth ranges, collapses averaged profiles in ACT and PCT to within a factor of 2.

2 Measurements

The measurements discussed here were made from sensors deployed on equatorial moorings at 0°140°W, part of the TAO/TRITON array in the Pacific (McPhaden et al., 1998) and at 0°23°W and 0°10°W, part of the PIRATA array in the Atlantic (Bourlès et al., 2019).

Besides the χpod turbulence measurements, the analysis employs (i) temperature profiles from the main moorings on which the χpods are deployed to determine the time-varying stratification and (ii) velocity data from nearby subsurface moorings outfitted with upward-looking acoustic Doppler current profilers (ADCPs). A complete analysis primer (Warner, 2020) describes how the temperature variance dissipation rate (χ), the turbulence kinetic energy dissipation rate (ϵ) and the turbulence diffusivity (K_T) are computed from high frequency temperature measurements using fast thermistors on χpods with speed and stratification inputs from the moored temperature and velocity data (Moum & Nash, 2009; Zhang & Moum, 2010; Perlin & Moum, 2012).

We began deploying χpods on the TAO/TRITON mooring at 0°140°W in September 2005 and have attempted to maintain these measurements continually. In 2014, we began deployments of χpods at 0°10°W and 0°23°W. The full records from all χpods at each location are shown in Figure 1.

3 Common features of ϵ in ACT and PCT

From an 8-day record of shipboard profiling measurements at 0°140°W, Smyth and Moum (2013) showed that there exists a depth range between ML base and EUC core (where zonal current shear vanishes; Figure 2b) over which N^2 and Sh^2 interact in such

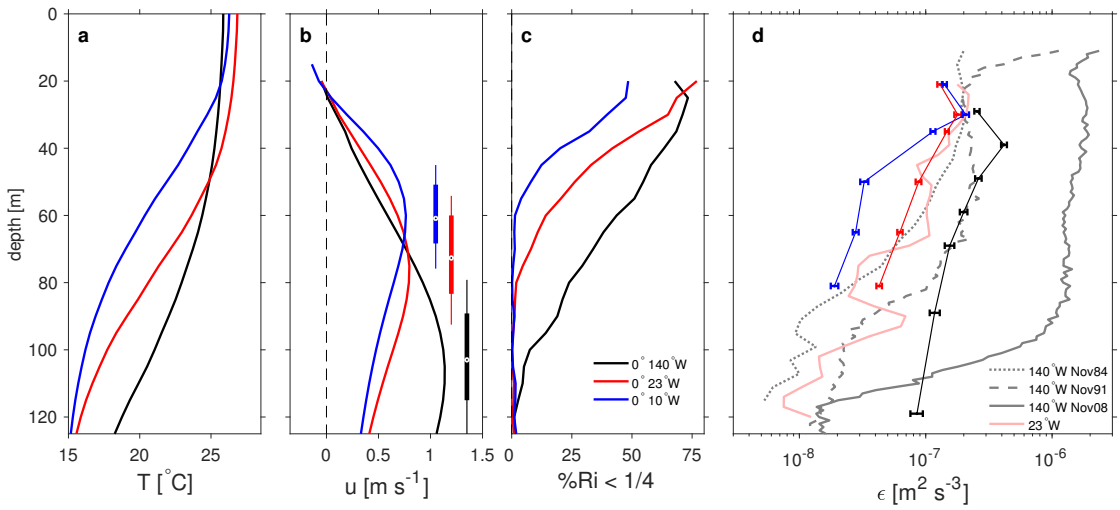

Figure 2. Averaged vertical profiles at the equator in the ACT (10°W, 23°W; 2013–2019) and PCT (140°W; 2005–2019). a) temperature (T); b) zonal velocity (u) with the depth of the EUC core (where $u_z \rightarrow 0$) indicated by vertical bars (25th and 75th percentiles are thick bars and 10th and 90th percentiles are thin bars; statistics from hourly averages). Full current profiles in (b) were constructed with the aid of current meters deployed on the surface mooring to fill in above the upper ADCP range limit at about 40 m depth.; c) statistic indicating the percentage of time that the gradient Richardson number, Ri, is less than 1/4 as determined from hourly data; d) mean values of turbulence dissipation rate, ϵ, from χpods with 95% confidence limits computed using non-parametric bootstrap statistics on hourly-averaged data. Averaged vertical profiles are from shipboard experiments at 0°140°W in 1984 (Tropic Heat - 1749 profiles over 12 consecutive days; Moum et al. (1989)), 1991 (Tropical Instability Wave Experiment - 3918 profiles over 22 consecutive days; Lien et al. (1995)) and 2008 (2624 profiles over 16 consecutive days) (Moum et al., 2009); averages of 154 vertical profiles (red) at 0°23°W taken over 5 mooring deployment cruises during the period 2008–2016, roughly split between boreal spring and boreal autumn (Dengler & Mehrtens, 2021). Note that estimates of ϵ for the profiling measurements are derived from shear probe measurements and for the χpods from fast thermistor measurements following Moum and Nash (2009); Zhang and Moum (2010).

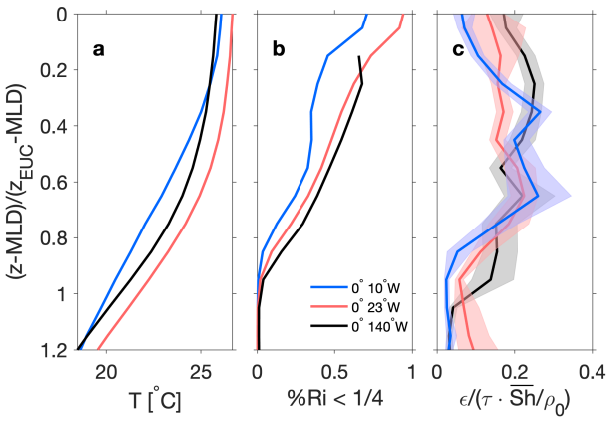

Figure 3. Vertical profiles scaled such that the DC layer, from the ML base to the EUC core depth, ranges over 0–1. Scalings employ daily-averaged data. z = -depth and $z > 0$, upward; MLD is the base of the ML; z_{EUC} is the EUC core depth. (a) T; (b) percentage of values with $Ri < 1/4$; (c) ϵ scaled by the product of the wind stress (τ) and $\overline{Sh}$, the average value of Sh over the DC layer, divided by the mean density, ρ_0. Note the abscissa of (c) is a linear scale. Shading indicates 95% bootstrap confidence limits.

a manner that $Ri = N^2/Sh^2$ fluctuates about a critical value, $Ri_{cr} = 1/4$. Here, $N^2 = -g\rho_z/\rho_0$ is the squared buoyancy frequency representing density stratification, where ρ is the depth-dependent density, ρ_0 is a background reference value, subscript z represents differentiation with respect to the vertical and g is Earth's gravitational acceleration. Squared current shear is defined as $Sh^2 = u_z^2 + v_z^2$, where u is the zonal and v the meridional component of velocity. A useful metric of instability is the percentage of hourly values that are less than Ri_{cr} (Figure 2c). At and below the mean depths of the EUC core there are very few values of $Ri < Ri_{cr}$. This is the case at all three locations (Figure 2c). Upward from the core depths, the frequency of occurrence of $Ri < Ri_{cr}$ increases, to 75% at 20 m at 140°W and 23°W, and 50% at 10°W. In each case, the 50% metric occurs at roughly 1/2 the distance from the EUC core depth to the sea surface. At 10°W, the depths where $Ri < Ri_{cr}$ occurs most frequently are likely shallower than 20 m and not sampled by the PIRATA velocity sensors and hence Ri is not computed there. The ranges of EUC core depths (based on hourly data) are deepest at 140°W and shallow from 23°W to 10°W (Figure 2b).

At the two Atlantic sites, the mean values of ϵ, ($\overline{\epsilon}$), are nearly identical at the two uppermost χpods (Figure 2d). At both, the maximum in $\overline{\epsilon}$ occurs at the second χpod at 30m. At 140°W the maximum value of $\overline{\epsilon}$ occurs at 40m. For each site, the decrease from the respective maxima of $\overline{\epsilon}$ to its value at EUC core depth is

- a factor of 10 at 10°W (EUC core at 61m);
- a factor of 6 at 23°W (EUC core at 73m); and
- a factor of 4 at 140°W (EUC core at 103m).

Commonalities in the vertical structure and magnitude of the statistic $\%Ri < 1/4$ are revealed by scaling the depth (where z = -depth) to isolate the DC layer such that the vertical coordinate is $(z-MLD)/(z_{EUC}-MLD)$, where MLD is the depth of the ML base and z_{EUC} is the EUC core depth (Figure 3b). Here and in the subsequent scaling of ϵ, daily data are first scaled and then bin-averaged in scaled depth.

Commonalities in the vertical structure and magnitude of ϵ are seen via scaling of ϵ by $\tau \cdot \overline{Sh}/\rho_0$, where τ is the surface wind stress, $\overline{Sh}$ is the mean value of Sh over the DC layer and ρ_0 a mean water density (Smyth et al., 2017). This scaling is equivalent to $u_*^2 \cdot \overline{Sh}$ where the friction velocity $u_* = \sqrt{\tau/\rho_0}$. Moum et al. (1989) found the mean value of $\epsilon/(\tau \cdot \overline{Sh}/\rho_0)$ to be about 0.2 from 12 days of profiling in 1984 at 0°140°W. In Figure 3a, these scalings neatly collapse the vertical profiles of ϵ from the three sites to within a factor of 2 at each scaled depth and close to the value of 0.2 found for the limited data set examined by Moum et al. (1989). Note that the model of pulsating DC turbulence derived by Smyth et al. (2017) pertains to night-time only and was tested using data between 20m and 70m depth in a regime of exceptionally strong DC, [November 2008 at 140W; see (Moum et al., 2009)]. In that case the scaled value was 0.86. In contrast, the present test uses long-term averages and therefore includes many times when the DC turbulence is expected to be weak or absent, e.g., daytime and spring minima (Pham et al., 2017; Smyth et al., 2021). The present value 0.2 is therefore more representative of the climatology of the cold tongues.

A surprising result from these averaged profiles is that long term mean values of ϵ are close to those values from short shipboard experiments executed in the absence of tropical instability waves (TIWs) in 1984 and 1991 (Figure 2d) and an order of magnitude smaller than the 2008 measurements made during the passage of a TIW (shown in Figure 2d as the solid grey line). This suggests that the influence of TIW-induced mixing on long term means is less than expected from the measurements made in 2008 (Moum et al., 2009; Inoue et al., 2012, 2019). The time period of the 2008 experiment is included in the mean χpod estimates of ϵ shown in Figure 2d. Confidence in these measurements is justified by previous comparisons between 16-day averages of ϵ from (i) shipboard profiling (using shear probes) and (ii) multiple χpods on both the TAO mooring and an additional nearby mooring that showed agreement to within a factor of 2 (Perlin & Moum, 2012).

4 Diurnal variability in ACT and PCT

The existence and behavior of DC turbulence at the equator and 140°W has been well-established through a series of short shipboard profiling investigations there (Moum & Caldwell, 1985; Gregg et al., 1985; Moum et al., 1989; Lien et al., 1995; Smyth et al., 2013). However, details of the averaged vertical structure and indeed the magnitudes of the DC turbulence differed between these necessarily short experiments (Figure 2d). Here we examine diurnal variations in the DC layer using several years of data from χpods at our three locations.

Ensembles of 10-minute averaged values of ϵ, measured at the uppermost χpod, were binned at 10-minute intervals in local time over 24 hours, centered at midnight. Our analysis is intended to reference solar time. On an annual basis, local time differs from solar time by at most 17 minutes at the equator: sunrise occurs at 06:00 local time ±17 minutes and sunset at 18:00 local time ±17 minutes, the variations being due to the combined effects of Earth's axial tilt and the eccentricity of its orbit, quantified by the equation of time (D. W. Hughes et al., 1989). With 10 minute bins, annual variations in solar time relative to local time are less than two bins and use of local time is therefore adequate for the purpose at hand.

Because computation of ϵ involves division by T_z (Moum & Nash, 2009), estimation is avoided for small, uncertain values of T_z and the data were originally selected by flagging intervals with small values of T_z (< 0.001 K m^{-1}) as would occur in the ML. At 29 m depth and 0°140°W the data consists of 242,879 independent 10-minute intervals representing 1,686 days (Figure 4b). Due to flagging for small values of T_z, fewer data points are found at times later in the night when the ML infrequently descends to 29 m at the Pacific location (Figure 4c) and somewhat earlier to 21 m at the Atlantic

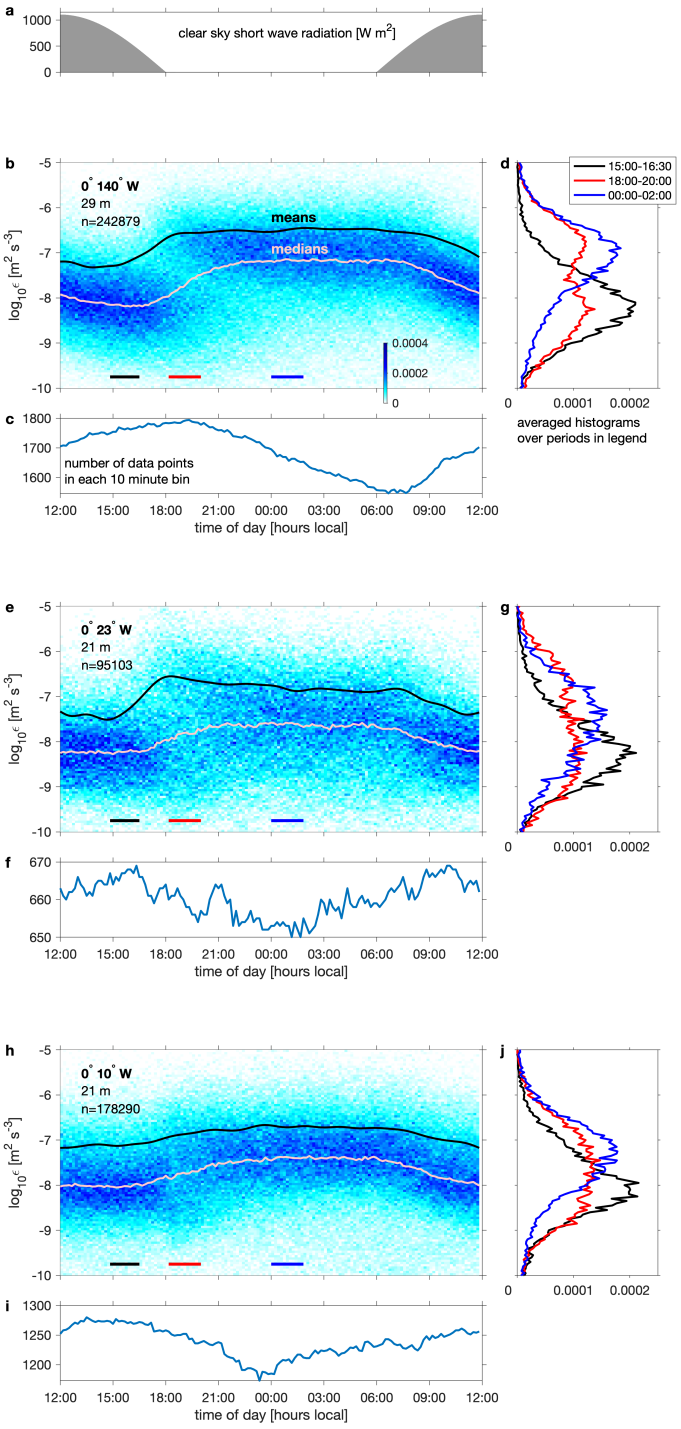

Figure 4. (a) Clear sky short wave radiation to solar time; (b,e,h) Diurnally-sorted probability distributions of $\log_{10}\epsilon$ (increments logarithmically spaced at 0.05) from the uppermost χpod records at the equator and 140°W (b), 23°W (e) and 10°W (h). Black/grey curves represent mean/median values for each 10 minute time interval. The value n at upper left is the number of 10 minute intervals represented. (c,f,i) number of data points in each 10 minute time interval. (d,g,j) One-dimensional histograms of ϵ computed by averaging over the time intervals shown in the legend and indicated by the colored bars at the bottom of (b,e,h).

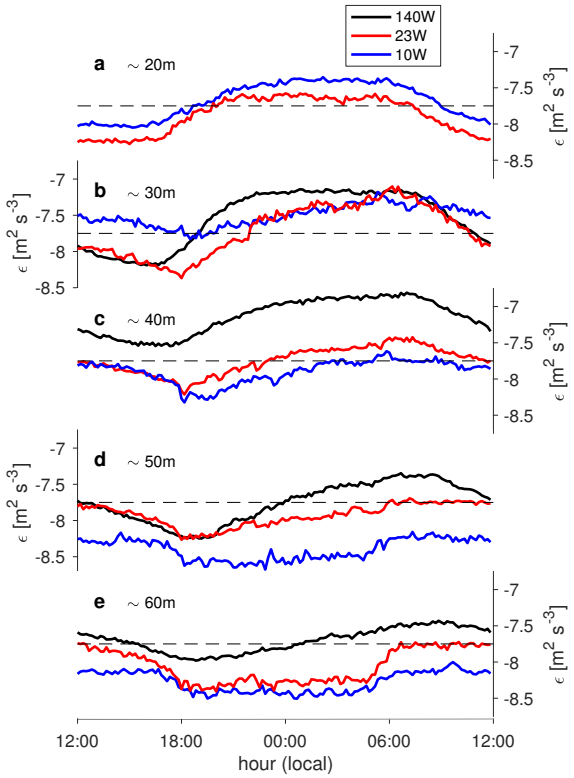

Figure 5. Median values of ϵ at 20 to 60 m depth as a function of local time. The two series at 20 m represent the uppermost χpods at 10°W and 23 °W and replicate the median lines in Figure 4e,h. The black series at 30 m (the uppermost χpod at 140°W) replicates the median line in Figure 4b. The depths shown here are within 5 m of deployed depths.

sites (Figure 4f,i). The uppermost χpods at all three locations are significantly deeper than the 90^{th} percentile of ML depths.

Systematic diurnal changes are clear in the variability of ϵ at 0°140°W as indicated by the progression of the cloud of points representing the time-dependent probability distributions in Figure 4b. There is a general decrease in ϵ beginning after sunrise and continuing to sunset. Around sunset, there is an impulse-like increase in ϵ from daytime values to a range of values that remains relatively steady until sunrise. Day to night increases of both means and medians are about a factor of 10. Modes differ by more than a factor of 10 (Figure 4d) as indicated by the averaged distributions of ϵ before (black - 15:00-16:30) and after (blue - 00:00-02:00) the sunset transition.

This general pattern of diurnal variation of ϵ is repeated at both the 23°W and 10°W sites (Figures 4e-i). Daytime values are roughly the same as at the 140°W site. Nighttime values are smaller at 10°W and 23°W (Figure 5). At 30 m depth (typically near the uppermost extent of the DC), the sharp day to night transition in mean values of ϵ at 23°W is similar to that at 140°W and less so at 10°W. The diurnal variation of the median value of ϵ is apparent at all three sites at all depths to 60 m (Figure 5). With increasing depth, the transition to larger nighttime values is delayed in time and reduced in magnitude, which is consistent with DC turbulence being a cycle triggered by surface changes.

At both PCT and ACT locations, distributions of 10-minute averages taken at the uppermost χpods show the dominance of low values in the afternoon, high values after

midnight, and a broad, nearly bimodal combination of both during the transition (Figure 4, 18:00 – 20:00). Elsewhere, we show that this apparent bimodal structure is largely associated with an additional dependence on the magnitude of the local wind stress that controls the timing of the transition (Moum et al., 2022).

5 Conclusions

The 15 years of χpod measurements at 0°140°W provide a different perspective of DC turbulence from the short shipboard experiments previously executed there. Most importantly, they show DC turbulence to be a robust feature that clearly stands out over the multiyear record (Figure 4).

This manuscript describes our first comprehensive look at the χpod records from the ACT. Comparisons to measurements from the PCT at 0°140°W shows the sites at 0°10°W and 0°23°W to exhibit the salient characteristics of the diurnal cycle of turbulence beneath the ML that we associate with DC turbulence. That is, at all three sites, the turbulence extends below the ML base and cycles diurnally (properties 1 and 2 listed in the Introduction). These comparisons also show the averaged magnitudes of ϵ near the base of the ML (nominally 30m) to be consistent within a factor of two at the three sites. While depth dependence varies considerably, the comparisons also support a depth scaling that isolates the relative deep cycle layers with scaling of ϵ by $\tau \cdot \overline{Sh}/\rho_0$. This combination of depth and amplitude scalings collapses the measurements at the three sites to within a factor of 2 at all depths.

The diurnal composite distributions of Figure 4 indicate that the temporal structure of DC turbulence is a persistent feature at all of the sites, and the scalings indicate a consistency between them. This should provide some confidence that DC turbulence is a persistent and consistent feature of the cold tongues in general. While features of DC turbulence have been simulated by Pei et al. (2020) in a global ocean general circulation model, quantification of the full zonal and meridional extent of DC turbulence via direct measurement remains an outstanding and important task.

Acknowledgments

The measurements described here have been fully funded by the National Science Foundation (grants 1256620, 1431518, 2048631). We acknowledge the efforts of past and present Ocean Mixing Group engineers M. Neeley-Brown, R. Kreth, A. Perlin, M. Borgerson, C. Van Appledorn, P. Vutukur, K. Latham and J. Logan in building, testing and calibrating χpods. We are grateful for the assistance of NOAA's National Data Buoy Center who deploy and recover instruments on the TAO/TRITON array and to NOAA's Pacific Marine Environmental Lab who coordinate shipments including our χpods to IRD (France) for deployment and recovery of the instruments on the PIRATA array and to IRD's "IMAGO unit", led by Fabrice Roubaud and Pierre Rousselot, who direct the mooring and χpod deployments for French Pirata cruises. WDS and JNM acknowledge support from the National Science Foundation under grant 1851520. PB and MD acknowledge support from the EU H2020 program (grants 817578 TRIATLAS and 101003470 NextGEMS).

The χpod data, ancillary data, mooring details and history are available at NOAA's Global Tropical Moored Buoy Array - https://www.pmel.noaa.gov/gtmba/.

References

Anis, A., & Moum, J. N. (1994). Prescriptions for heat flux and entrainment rate in the upper ocean during convection. *J. Phys. Oceanogr.*, *24*, 2142–2155.

Bourlès, B., Araujo, M., McPhaden, M. J., Brandt, P., Foltz, G. R., Lumpkin, R.,

& et.al. (2019). Pirata: A sustained observing system for tropical atlantic climate research and forecasting. *Earth and Space Science*, *6*, 577–616. doi: 10.1029/2018EA000428

Dengler, M., & Mehrtens, H. (2021). Data from: Sfb754 turbulence measurements (mss). *WorldData Center*. doi: 10.1594/PANGAEA.926518

Dohan, K., & Davis, R. E. (2011). Mixing in the transition layer during two storm events. *J. Phys. Oceanogr.*, *41*, 42-66.

Gregg, M. C., Peters, H., Wesson, J. C., Oakey, N. S., & Shay, T. J. (1985). Intensive measurements of turbulence and shear in the Equatorial Undercurrent. *Nature*, *318*, 140-144.

Hughes, D. W., Yallop, B., & Hohenkerk, C. (1989). The equation of time. *Mon. Not. R. Astr. Soc.*, *238*, 1529–1535.

Hughes, K. G., Moum, J. N., Shroyer, E. L., & Smyth, W. D. (2021). Stratified shear instabilities in diurnal warm layers. *J. Phys. Oceanogr.*. doi: 10.1175/JPO-D-20-0300.1

Hummels, R., Dengler, M., & Bourlès, B. (2013). Seasonal and regional variability of upper ocean diapycnal heat flux in the Atlantic cold tongue. *Prog. Oceanogr.*, *111*, 52-74. doi: 10.1016/j.pocean.2012.11.001

Hummels, R., Dengler, M., Rath, W., Foltz, G., Schutte, F., & Brandt, P. (2020). Surface cooling caused by rare but intense near-inertial wave induced mixing in the tropical Atlantic. *Nature Comm.*, *43*. doi: 10.1038/s41467-020-17601-x

Inoue, R., Lien, R.-C., & Moum, J. N. (2012). Modulation of equatorial turbulence by a tropical instability wave. *J. Geophys. Res. Oceans*, *117*. doi: 10.1029/2011JC007767

Inoue, R., Lien, R.-C., Moum, J. N., Perez, R. C., & Gregg, M. C. (2019, Mar). Variations of equatorial shear, stratification, and turbulence within a tropical instability wave cycle. *J. Geophys. Res. Oceans*, *124*(3), 1858–1875. doi: 10.1029/2018JC014480

Lien, R., Caldwell, D. R., Gregg, M. C., & Moum, J. N. (1995). Turbulence variability in the central Pacific at the beginning of the 1991–93 El Nino. *J. Geophys. Res.*, *100*, 6881-6898. doi: 10.1029/94JC03312

McPhaden, M., Busalacchi, A., Cheney, R., Donguy, J.-R., Gage, K., nd M. Ji, D. H., ... Takeuchi, K. (1998). The tropical ocean-global atmosphere observing system: A decade of progress. *J. Geophys. Res.*, *103*, 14169–14240. doi: 10.1029/97JC02906

Moum, J. N., & Caldwell, D. R. (1985). Local influences on shear flow turbulence in the equatorial ocean. *Science*, *230*, 215–315.

Moum, J. N., Caldwell, D. R., & Paulson, C. A. (1989). Mixing in the equatorial surface layer and thermocline. *J. Geophys. Res.*, *94*, 2005–2021. doi: 10.1029/JC094iC02p02005

Moum, J. N., Hughes, K. G., Shroyer, E. L., Smyth, W. D., Cherian, D., Warner, S. J., ... Dengler, M. (2022). Wind dependencies of deep cycle turbulence in the equatorial cold tongues. *Journal of Physical Oceanography*, submitted.

Moum, J. N., Lien, R.-C., Perlin, A., Nash, J. D., Gregg, M. C., & Wiles, P. J. (2009). Sea surface cooling at the equator by subsurface mixing in tropical instability waves. *Nat. Geosci.*, *2*, 761-765. doi: 10.1038/ngeo657

Moum, J. N., & Nash, J. D. (2009). Mixing measurements on an equatorial ocean mooring. *J. Atmos. Oceanic Technol.*, *26*, 317–336. doi: 10.1175/2008JTECHO617.1

Pei, S., Shinoda, T., Wang, W., & Lien, R.-C. (2020). Simulation of deep cycle turbulence by a global ocean general circulation model. *Geophys. Res. Lett.*, *47*. doi: 10.1029/2020GL088384

Perlin, A., & Moum, J. N. (2012). Comparison of thermal variance dissipation rates from moored and profiling instruments at the equator. *J. Atmos. Oceanic Technol.*, *29*, 1347–1362. doi: 10.1175/JTECH-D-12-00019.1

Pham, H. T., Smyth, W. D., Sarkar, S., & Moum, J. N. (2017). Seasonality of deep cycle turbulence in the eastern equatorial pacific. *J. Phys. Oceanogr.*, *47*, 2189–2019. doi: 10.1175/JPO-D-17-0008.1

Shay, T. J., & Gregg, M. C. (1986). Convectively driven turbulent mixing in the upper ocean. *J. Phys. Oceanogr.*, *16*, 1777–1798.

Smyth, W. D., & Moum, J. N. (2013). Marginal instability and deep cycle mixing in the eastern equatorial Pacific Ocean. *Geophys. Res. Lett.*, *40*, 6181-6185. doi: 10.1002/2013GL058403

Smyth, W. D., Moum, J. N., Li, L., & Thorpe, S. A. (2013). Diurnal shear instability, the descent of the surface shear layer and the deep cycle of equatorial turbulence. *J. Phys. Oceanogr.*, *43*, 2432-2455. doi: 10.1175/JPO-D-13-089.1

Smyth, W. D., Pham, H., Moum, J. N., & Sarkar, S. (2017). Pulsating stratified turbulence in the upper equatorial oceans. *J. Fluid Mech.*, *822*, 327-341. doi: 10.1017/jfm.2017.283

Smyth, W. D., Warner, S. J., Moum, J. N., Pham, H., & Sarkar, S. (2021). A proxy for equatorial deep cycle turbulence and its variation over multiple enso cycles. *J. Phys. Oceanogr.*, *51*, 2291-2302. doi: https://doi.org/10.1175/JPO-D-20-0236.1

Warner, S. J. (2020). χpod and GusT Processing Manual. *Oregon State University*.

Warner, S. J., & Moum, J. N. (2019, Dec). Feedback of mixing to ENSO phase change. *Geophys. Res. Lett.*, *46*(23), 13920–13927. doi: 10.1029/2019gl085415

Zhang, Y., & Moum, J. N. (2010). Inertial-convective subrange estimates of thermal variance dissipation rate from moored temperature measurements. *J. Atmos. Oceanic Technol.*, *27*, 1950–1959.